# Experimental and Theoretical $NO_x$ Physisorption Analyses of Mesoporous Film (SBA-15 and SBA-16) Constructed Surface Photo Voltage (SPV) Sensor

**Takeo Yamada,[†] HaoShen Zhou,*[,†] Hidekazu Uchida,[§] Itaru Honma,[†] and Teruaki Katsube[§]**

*Energy Electronics Institute, National Institute of Advanced Industrial Science and Technology (AIST), AIST Tsukuba Central 2, 1-1-1 Umezono, Tsukuba, Ibaraki 305-8568, Japan and Department of Information and Computer Science, Faculty of Engineering, Saitama University, 255 Shimo-okubo, Saitama, Saitama 338-0825, Japan*

*Received: March 31, 2004; In Final Form: June 21, 2004*

Mesoporous silica films with hexagonal (SBA-15) and cubic (SBA-16) mesostructures have been successfully employed to fabricate surface photo voltage (SPV) sensors for $NO_2$ gas. These SPV sensors exhibited better sensitivity (*S*) in 50 ppm $NO_2$ gas than in 100 ppm NO gas. SPV with SBA-16 film showed better sensitivity in 1 ppm $NO_2$ gas than in 1 ppm NO gas. These phenomena can be explained by the physical adsorption of the target gas into the mesoporous layer, which is regarded as the insulator layer in metal−insulator-semiconductor (MIS) devices.

## Introduction

The problem of environmental pollution, especially of air pollution, remains serious. In particular, nitrogen oxides, which are emitted by various combustion processes, both act as a source of acid rain and cause serious damage to human health. All nations have therefore regulated and limited the concentrations of these gases in air by imposing legal controls on automotive and industrial emissions. Accordingly, there is an urgent need for the development of a highly sensitive, highly responsive, and portable detection device for monitoring these gases.[1−3] However, almost all conventional detection systems are too large and have too-complicated operating procedures to be used as in situ monitoring detectors. We recently applied self-ordered mesoporous silica films, hexagonal (SBA-15) and cubic (SBA-16),[4] to an NO gas sensor that exploits the surface photo voltage (SPV) semiconductor characterization technique.[5−7] The large surface area and uniform nanosize pores of self-ordered mesoporous materials enable SPV devices to show good gas adsorption properties with better sensitivity and selectivity. These self-ordered mesoporous silica films were synthesized by spin coating using a nonionic poly(ethylene oxide)−poly(propylene oxide)−poly(ethylene oxide) (PEO−PPO−PEO)-type triblock copolymer surfactant as the structure-directing agent.

The basic principle of the SPV technique is based on the semiconductor surface potential property of the metal−insulator-semiconductor (MIS) structure.[8−10] The self-ordered mesoporous silica film, which was coated on a semiconductor n-Si substrate, was used as an insulator layer for a special capacitor. The change in capacitance, which results from both the physical and the chemical adsorption of the target gas onto the inner surface of the mesoporous layer, could be detected by an alternating photocurrent (AC) that was excited by a light-emitting diode (LED).[5−7,9] Notably, the capacitance of this MIS device depended on the pore size, mesostructure, and morphology of the self-ordered mesoporous silica films, allowing the improvement of these parameters to lead directly to enhancement of the SPV gas sensor's characteristics.[5−7]

In this paper, we report the $NO_2$ gas (1 and 50 ppm) detection properties of the SPV system. The self-ordered mesoporous SPV sensor shows different sensing properties for NO and $NO_2$ gas.[5−7] These results are from the difference in dielectric constant between NO and $NO_2$, both of which are adsorbed onto the inner surface of mesopores in the self-ordered mesoporous film. This phenomenon of sensing properties that vary depending on the mesostructure, which is found in the NO SPV sensor, is also observed in the $NO_2$ SPV sensor.

## Experimental Section

**Materials.** Homogeneous and transparent mesoporous silica films are synthesized by spin coating, using a nonionic PEO−PPO−PEO triblock copolymer surfactant as the structure-directing agent.[4,11−13] The precursor for the coating sol solution is prepared from two solutions. One is a polymer solution, containing the template triblock copolymer dissolved in ethanol (EtOH). The other is a silica solution, which contains a mixture of tetraethyl orthosilicate (TEOS), EtOH, distilled water, and hydrochloric acid. These polymer and silica solutions are mixed and used to coat the sol solution. The mole ratio of chemicals of the coating sol solution was TEOS:$EO_{20}PO_{70}EO_{20}$ (P123):$H_2O$:HCl:EtOH = 1:0.014:15:0.16:39 for a self-ordered hexagonal structured SBA-15 film and TEOS:$EO_{100}PO_{65}EO_{100}$ (F127):$H_2O$:HCl:EtOH = 1:0.041:15:0.16:40 for a self-ordered cubic structured SBA-16 film. The coating sol solution is employed to spin coat a film onto a substrate. Finally, calcination is carried out at 450 °C for 12 h to remove the triblock copolymer template and obtain homogeneous and transparent mesoporous silica films.

Figures 1(a) and 1(b), respectively, show X-ray diffraction (Material Analysis and Characterization Science Co., Ltd.: XRD M03XHF22) patterns and transmission electron micrograph (JEOL, Ltd.: JEM-2010F) images of SBA-15 and SBA-16 self-ordered mesoporous silica film.[6] In Figure 1(a), three peaks, which have a *d* spacing ratio of 1:1/2:1/3, are observed

* E-mail: hs.zhou@aist.go.jp, Fax: +81-29-8615829.
[†] National Institute of Advanced Industrial Science and Technology.
[§] Saitama University.

10.1021/jp048597i CCC: $27.50 
Published on Web 08/06/2004

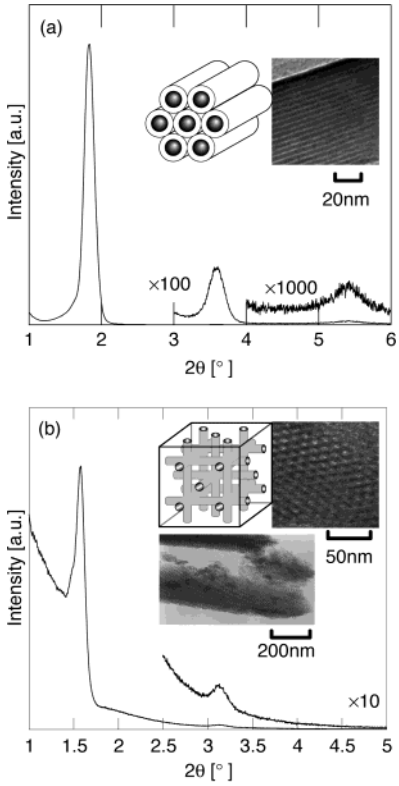


**Figure 1.** XRD pattern, TEM image (inset) and graphical image (inset) of self-ordered mesoporous films: (a) the XRD pattern and images of the SBA-15 film, (b) the XRD pattern and images of the SBA-16 film.

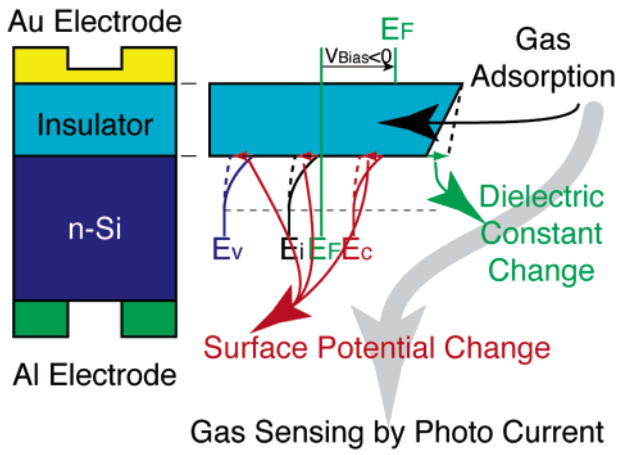


**Figure 2.** Structure (left) and band diagram (right) of the SPV device.

in the calcined sample. They can be indexed, respectively, as the (100), (200), and (300) reflections of a two-dimensional hexagonal (2DH) structure.[4,11−13] According to the TEM image, the film has a highly oriented 2DH structure, and the pore channel is parallel to the substrate surface. This orientation along the plane causes the disappearance of the (110) and (210) reflections of the hexagonal structure in the XRD pattern.

In Figure 1(b), two peaks, with a *d* spacing ratio of 1:1/2, are observed. Although it is difficult to decide the structure of the film, it can be observed in the TEM image that the pores have a three-dimensional structure. Hence, the film is evaluated as a cubic structure.[6,7]

**Principle of SPV.** Figure 2 shows the constitution of the SPV sensor that comprises the MIS structure of Au/mesoporous silica (self-ordered hexagonal or cubic structure)/$Si_3N_4$/$SiO_2$/n-Si/Al.

The principle of the self-ordered mesoporous film SPV gas sensor has been reported.[5] A direct current (DC) bias voltage is applied between the Au and Al electrode in SPV systems. An LED, to which is applied a 1-kHz AC current, is employed to irradiate the n-Si substrate to excite photoelectrons and holes. Figure 2 also shows the energy band gap diagram of the MIS structure and, in brief, the principle of gas detection. There are three typical cases of the semiconductor surface band diagram that depend on the bias voltage ($V_B$). The first is accumulation of electrons ($\phi_s > 0$), the second is depletion of electrons ($\phi_B < \phi_s < 0$), and the third is inversion ($\phi_s < \phi_B$). Here, $\phi_s$ and $\phi_B$ are, respectively, the surface potential and the potential difference between the Fermi level ($E_F$) and the intrinsic Fermi level ($E_i$).[10] Basic relations among the bias voltage $V_B$, surface potential, and surface charge are described by the following equation.

$$V_B = \phi_S - \frac{Q_S + Q_0}{C_i} \quad (1)$$

Here, $C_i$ is the insulator capacitance, including the capacitances of the mesoporous silica film, the $Si_3N_4$ layer, and the substrate $SiO_2$ layer. $Q_S$ is the surface charge. The total charge, $Q_o$, includes oxide fixed charge, net mobile ions, and oxide-trapped charge.

According to the equation, the surface voltage depends strongly on the insulator capacitance. The dielectric constant, and the oxide-trapped charge of the insulator change after the target gas, is adsorbed onto the inner surface of the self-order mesoporous silica layer. These changes in both the dielectric constant and the charge produce changes in the capacitance $C_i$ and the AC that is detected as a sensor signal as shown in Figure 2.[5]

## Results and Discussion

Figure 3(a) shows both the bias voltage-current curve (BC-curve) and the bias voltage-alternating photocurrent phase curve (BP-curve) for the SPV device with a self-ordered hexagonal-structured SBA-15 film (SPV-hex), measured at room temperature under standard air exposure conditions ($O_2$: 20%, $N_2$: 80%, 100 sccm) and $NO_2$ gas exposure conditions (50 ppm, 100 sccm). A clear bias voltage shift can be observed after the exposure to the 50-ppm $NO_2$ gas. Recoverable responses of both photocurrents and the phase of SPV-hex with measurement time at a bias voltage of 1.1 V, under cyclic gas flowing between the standard air and the 50-ppm $NO_2$ gas, are also shown in Figure 3(b). The photocurrent increases cyclically with turning on the $NO_2$ gas and decreases with turning off the $NO_2$ gas (equals standard air turning on). Simultaneously, the phase of the photocurrent decreases cyclically with turning on the $NO_2$ gas and increases with turning off the $NO_2$ gas. This response time ranges from several tens to several hundreds of seconds, which results from the physical balance time of the adsorption−desorption process of the $NO_2$ gas at the surface of the mesopores.

In high cycle numbers, the response time appears to lengthen, which indicates there is some residual $NO_2$ gas in each removal cycle due to exposure to the standard air. This residual $NO_2$ gas causes poor cycle response of our SPV sensor. One way to remove the residual $NO_2$ gas in each cycle is to increase the operating temperature from room temperature to 80 °C or 100 °C. The problems caused by humidity and water in the air can be also solved by increasing the operating temperature. This procedure is currently being optimized. A BC-curve and a BP-curve of the SPV device with the self-ordered cubic structure silica film (SPV-cub) in 50-ppm $NO_2$ are shown in Figure 3(c).

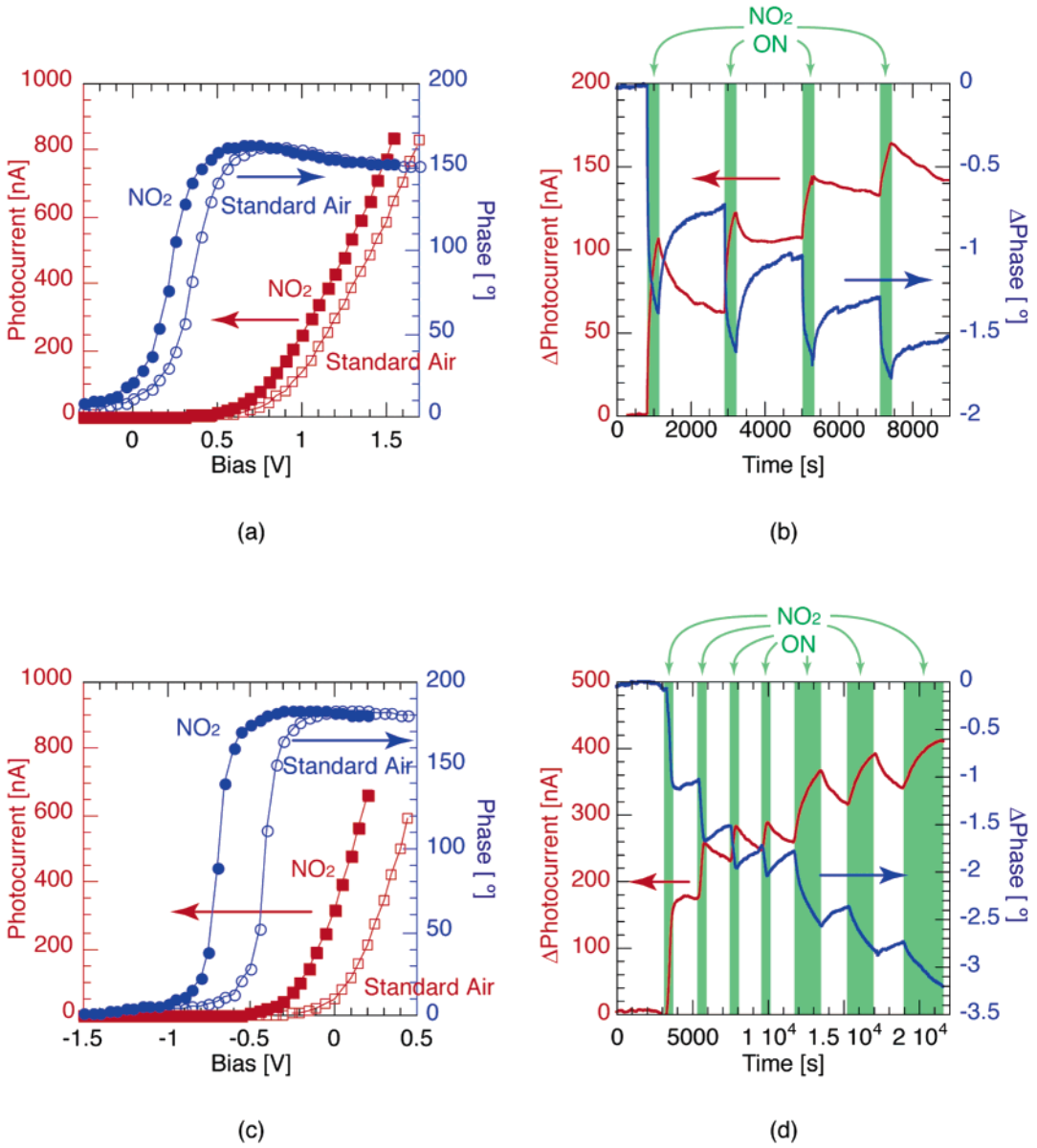


**Figure 3.** 50 ppm $NO_2$ exposure results for SPV-hex and SPV-cub: (a) BC-curve and BP-curve of SPV-hex, (b) photocurrent and phase response of SPV-hex at 1.1 V bias voltage, (c) BC-curve and BP-curve of SPV-cub, and (d) photocurrent and phase response of SPV-cub at 0.15 V bias voltage. Here, red and blue, respectively, signify photocurrent and phase properties. Open squares and circles indicate standard air exposure, and closed squares and circles indicate 50 ppm $NO_2$ exposure. The green and white areas of (b) and (d) indicate, respectively, 50 ppm $NO_2$ exposure and standard air exposure.

Recoverable responses of both photocurrent and its phase of SPV-cub with measurement time at a bias voltage 0.15 V, under cyclic gas flowing between the standard air and the 50-ppm $NO_2$ gas at room temperature, are also shown in Figure 3(d). In SPV-cub, the photocurrent is also alternately increased and decreased according to the cycle of exposure to the 50-ppm $NO_2$ and to the standard air. At the same time, the phase is decreased and increased according to the cycle of exposure as shown in Figure 3(d).

In SPV-hex, the bias shift due to 50-ppm $NO_2$ exposure is estimated at 149 mV at a photocurrent of 400 nA from the BC-curve and at 141 mV in 90° AC phase from the BP-curve.

In the BC-curve, the bias shift is estimated from the depletion region of the SPV device according to the bias voltage. On the other hand, in the BP-curve the bias shift is evaluated in the border area from the inversion region to the depletion region. Almost the same bias shift value can be obtained from both the BC-curve and the BP-curve, even in different regions, as shown in Figure 4. This indicates that a reasonable surface potential shift, which results from the target $NO_2$ gas adsorption, controls the SPV performance over a large potential range from the inversion case to the depletion case.

In SPV-cub, the bias shift caused by exposure to 50-ppm $NO_2$ is also estimated at 282 mV at a photocurrent of 400 nA from the BC-curve. It is also exactly the same, at 282 mV in 90° AC phase, as the BP-curve. These results indicate that the SPV devices have a sensing and recoverable property for $NO_2$ gas.

A comparison of the bias shift properties of SPV-hex with those of SPV-cub in the BC-curve and the BP-curve of the 50-ppm $NO_2$ gas shows that the inherent mesostructure of each mesoporous film influences SPV properties according to the same phenomenon as reported for the NO gas sensor.[7] SPV-cub gives a much larger bias voltage shift than that of SPV-hex, although the surface area of SBA-16 is similar to that of SBA-15, which is used in SPV-hex.

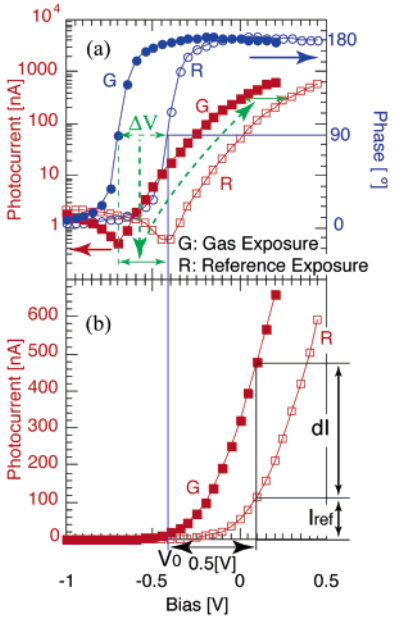


**Figure 4.** Expression defining sensitivity (*S*). (a) BC-curve against log photocurrent and BP-curve of SPV-cub for the definition expression of *S* and for the indication of the depletion region bias shift ($\Delta V$). (b) BC-curve of SPV-cub for the definition expression of *S*. Here, red and blue, respectively signify photocurrent and phase properties. Open squares and circles indicate reference gas exposure, and closed squares and circles indicate target gas exposure. $V_0$ is defined as the turning point from the depletion region to the inversion region of reference gas exposure, signified by 90° in the phase of the reference gas. d*I* and $I_{ref}$ are defined at $V_0 + 0.5$ [V]. *S* is also defined by $dI/I_{ref}$.

Here, we introduce the sensor sensitivity *S*, which is defined as

$$S = \frac{dI}{I_{ref}} \tag{2}$$

$$dI = I_{gas} - I_{ref} \tag{3}$$

where $I_{gas}$ and $I_{ref}$ are photocurrents measured at $V_0 + 0.5$ (V), in the exposure gas and the reference gas, respectively. The bias voltage at 90° in the phase of the reference gas is $V_0$, which marks the turning point from the depletion region to the inversion region, as shown in Figure 4 (a).

Figure 4 also shows the definition of sensor sensitivity (*S*). This is evaluated at a bias of $V_0 + 0.5$ (V), which is the depletion region. Generally, all SPV-type sensors are evaluated in the depletion region.[8,9] According to this definition, the *S* of SPV-hex and SPV-cub for the $NO_2$ gas exposure are calculated to be 1.24 and 1.99, respectively. Hence, SPV-cub is more sensitive than SPV-hex with respect to $NO_2$ exposure.

In the case of SPV-hex, which has a 2DH mesostructure, the pore channels are aligned parallel to the substrate surface. The gas can gain access only from the side, but not from the top of the 2DH mesostructure mesoporous film. On the other hand, in the case of SPV-cub, the pore channels connect with each other in three dimensions. The gas can therefore gain access to the film from both the top and the sides of the mesoporous insulator layer. Since the top area is much greater than the side area, SPV-cub gives a much larger bias voltage shift and S than SPV-hex.

The bias shift results of 100-ppm NO exposure are summarized in Table 1.[6] The bias shifts caused by 50-ppm $NO_2$ exposure from the BC-curve and the BP-curve are about 3 to 5 times larger than those of 100-ppm NO exposure from the BC-curve and the BP-curve in SPV-hex, respectively. Also, the bias shift due to 50-ppm $NO_2$ exposure from both the BC-curve and the BP-curve are about 3 times greater than those of the 100-ppm NO exposure from both the BC-curve and the BP-curve in SPV-cub.

**TABLE 1: Bias Shift Results of SPV-hex and SPV-cub in 100 ppm NO Exposure**

| | SPV-hex | SPV-cub |
|---|---|---|
| from BC-curve | 31 mV | 110 mV |
| from BP-curve | 47 mV | 110 mV |

According to these results, $NO_2$ gas is about 3 to 5 times more detectable than NO gas, even when compared at low concentrations of $NO_2$.

The bias shift at the flat band of a SPV structure in eq 1 can be described as below when $\phi_s = 0$ is defined.[5]

$$\Delta V_B = \frac{Q_{0AD}}{C_{iAD}} - \frac{Q_0}{C_i} = \frac{Q_0 + \Delta Q_0}{\epsilon_i + \Delta\epsilon_i} d - \frac{Q_0}{\epsilon_i} d = \frac{\epsilon_i \Delta Q_0 - \Delta\epsilon_i Q_0}{\epsilon_i + \Delta\epsilon_i} \frac{d}{\epsilon_i} \tag{4}$$

Here, $\Delta Q_0$, $C_{iAD}$, and $\Delta\epsilon_i$ are the changes in charge density, the capacitance after having adsorbed a gas, and the dielectric constant, respectively. Also, $\epsilon_i$ and *d* are, respectively, the dielectric constant and the thickness of the insulator layer.

The bias shift is from the change in both the dielectric constant (due to the physical adsorption) and the charge (due to chemical interaction between the detected gas and the gas-sensitive film). If we assume that both NO and $NO_2$ gas are physically adsorbed onto the inner surface of the mesopores in SPV-hex and SPV-cub, in this physical adsorption case, $\Delta Q_0 = 0$ and the equation below describes the process.

$$\Delta V_{gas} = \frac{-\Delta\epsilon_{gas}}{\epsilon_i + \Delta\epsilon_{gas}} \cdot \frac{Q_0}{\epsilon_i} d = \frac{-\Delta\epsilon_{gas}}{\epsilon_i + \Delta\epsilon_{gas}} V_{flat} \tag{5}$$

Here, $V_{flat}$ is the bias voltage at the flat band,[10] and $\epsilon_i$ and $\Delta\epsilon_{gas}$ are the dielectric constant of the insulator layer under reference gas exposure and the change in the dielectric constant resulting from target gas exposure, respectively. Furthermore, the bias shift ratio of the $NO_2$ exposure to the NO exposure is calculated below.

$$\frac{\Delta V_{NO_2}}{\Delta V_{NO}} = \frac{\dfrac{\Delta\epsilon_{NO_2}}{\epsilon_i + \Delta\epsilon_{NO_2}}}{\dfrac{\Delta\epsilon_{NO}}{\epsilon_i + \Delta\epsilon_{NO}}} = \frac{\Delta\epsilon_{NO_2}}{\Delta\epsilon_{NO}} \frac{\epsilon_i + \Delta\epsilon_{NO}}{\epsilon_i + \Delta\epsilon_{NO_2}} \tag{6}$$

Here, we assume that the target gas is homogeneously and physically adsorbed onto the mesoporous layer. The dielectric constant of the gas-adsorbed insulator layer ($\epsilon_{ins}$) can then be defined as below.

$$\epsilon_{ins} = f(\epsilon_{total}, \alpha, \epsilon, \beta) = f(\epsilon, \beta) \tag{7}$$

Here, $\epsilon_{total}$ and $\alpha$ are, respectively, the dielectric constants of the naked insulator layer, which does not adsorb any gas, and the porosity of the insulator layer. These values should be constants in the same mesostructure SPV device. Also, $\epsilon$ and $\beta$ are the dielectric constant of the exposure gas and the condensation factor of the exposure gas on the inner surfaces of the

**TABLE 2: Dielectric Constants for Standard Air, NO, $NO_2$, and $N_2$**

| standard air | NO | $NO_2$ | $N_2$ |
|---|---|---|---|
| 1.000536 | 1.000593 | 1.001781 | 1.00548 |

mesoporous film, respectively. The dielectric constant of the exposure gas could be written as

$$\epsilon = (1 - C_{gas})\epsilon_{ref} + C_{gas}\epsilon_{gas} = \epsilon_{ref} + C_{gas}(\epsilon_{gas} - \epsilon_{ref}) = \epsilon_{ref} + \Delta C\epsilon_{gas-ref} \quad (8)$$

where $\epsilon_{ref}$ and $\epsilon_{gas}$ are, respectively, the dielectric constants of the reference gas (e.g., air or $N_2$) and the target gas (e.g., NO or $NO_2$). Here, $C_{gas}$ and $\Delta C\epsilon_{gas-ref}$ are, respectively, the concentration of the target gas and the dielectric constant difference between the reference gas and the exposure gas. Therefore, the dielectric constant difference between the gas adsorbed and the naked insulator layer is described as

$$\Delta\epsilon_{gas} = f(\epsilon_{ref} + \Delta C\epsilon_{gas-ref}, \beta_{ref} + \Delta\beta_{gas-ref}) - f(\epsilon_{ref}, \beta_{ref}) \ll f(\epsilon_{ref}, \beta_{ref}) \quad (9)$$

Here, $\beta_{ref}$ and $\Delta\beta_{gas-ref}$ are, respectively, the condensation factor of the reference gas and the condensation factor difference between the reference gas and the exposure gas. Hence, eq 6 could be approximated as

$$\frac{\Delta V_{NO_2}}{\Delta V_{NO}} \approx \frac{\Delta\epsilon_{NO_2}}{\Delta\epsilon_{NO}} = \frac{\frac{\partial f}{\partial\epsilon}(\epsilon_{ref}, \beta_{ref})\cdot\Delta C\epsilon_{NO_2-ref} + \frac{\partial f}{\partial\beta}(\epsilon_{ref}, \beta_{ref})\cdot\Delta\beta_{NO_2-ref}}{\frac{\partial f}{\partial\epsilon}(\epsilon_{ref}, \beta_{ref})\cdot\Delta C\epsilon_{NO-ref} + \frac{\partial f}{\partial\beta}(\epsilon_{ref}, \beta_{ref})\cdot\Delta\beta_{NO-ref}} \quad (10)$$

Furthermore, we assume the condensation factors of NO and $NO_2$ to be the same. Equation 10 can then be approximated to eq 11.

$$\frac{\Delta V_{NO_2}}{\Delta V_{NO}} \approx \frac{\Delta\epsilon_{NO_2}}{\Delta\epsilon_{NO}} \approx \frac{C_{NO_2}(\epsilon_{NO_2} - \epsilon_{ref})}{C_{NO}(\epsilon_{NO} - \epsilon_{ref})} \quad (11)$$

The bias shift ratio of $NO_2$ exposure to NO exposure is calculated to be 10.9, where $C_{NO}$ and $C_{NO_2}$ are 100-ppm (0.0001) and 50-ppm (0.00005), respectively. The dielectric constants of the target gases and reference gases (where the reference gas is air) are listed in Table 2.[14]

On the other hand, the sensor sensitivity ($S$) for the NO exposure of SPV-hex and SPV-cub can be estimated as being 0.20 and 0.91, respectively. The $S$ for the NO exposure in SPV-hex and SPV-cub are smaller than those for $NO_2$ exposure, as for SPV-hex and SPV-cub. These results indicate that self-ordered mesoporous SPV sensors are more sensitive to $NO_2$ gas.

Although the calculated result from eq 11 is slightly different from the experimental data, the experimental data of the bias shift ratio in SPV-hex are evaluated as 4.8 and 2.6 from the BC-curve and BP-curve, respectively. Also, the data in SPV-cub are estimated to be 2.6 from both the BC-curve and BP-curve. However, both the calculated result and the experimental data are in the same order. We believe that the difference is due to the contribution of the micropores of the mesoporous film. These kinds of mesoporous materials have micropores in addition to mesopores, which is indicated by the nitrogen adsorption desorption isotherms and their t-plot analysis (the results are shown in Table 3). The ratio of the micropore surface area to the total surface area is about 40% and 70% in SBA-15 and SBA-16 powder, respectively.[15−19] The pore size of the micropores is estimated at about 0.6−0.7 nm.[15−19]

**TABLE 3: Result of t-plot Analysis for SBA-15 and SBA-16 Powder**

| | total surface area | micropore surface area | contribution micropore surface area to total surface area |
|---|---|---|---|
| SBA-15 powder | 790 $m^2/g$ | 320 $m^2/g$ | ~40% |
| SBA-16 powder | 850 $m^2/g$ | 590 $m^2/g$ | ~70% |

If molecules of $NO_2$ gas are assumed to be adsorbed to the inner surfaces of the micropores following the pattern of Langmuir adsorption (monolayer adsorption), the diameter of the micropores should be larger than double the molecular diameter of $NO_2$. Micropores with a diameter of 0.6−0.7 nm are, in fact, about double the molecular size of $NO_2$ but are much larger than double NO's molecular size. This suggests that the number of $NO_2$ molecules adsorbed in the micropores would be much lower than that of NO molecules. This micropore effect makes the experimental value (ranging from 3 to 5) of the bias voltage ratio smaller than the theoretical value of 10.9.

On the other hand, in the mesostructure dependence, the bias shift of the BC-curve in SPV-cub is also about 4 times larger than that in SPV-hex for NO gas exposure. However, the bias shift of the BC-curve in SPV-cub is only about double that of SPV-hex for $NO_2$ gas exposure. This decreased bias voltage ratio of SPV-cub over SPV-hex for $NO_2$ gas exposure also results from the micropore effect. In fact, the surface area of the micropores in SBA-16 (cubic structure) is about 590 $m^2/g$, but that in SBA-15 (hexagonal structure) is about 320 $m^2/g$.

According to the NO and $NO_2$ sensing results for 100 and 50-ppm, respectively, SPV-cub is more suitable than SPV-hex for an NO and $NO_2$ gas sensor. Therefore, SPV-cub was employed to investigate the sensing properties of 1-ppm NO and 1-ppm $NO_2$ gas. To reduce sensitivity to gases other than $NO_x$ in this quite low-concentration exposure environment, pure nitrogen gas was adopted as the diluted gas and the standard gas. The practical concentration of the NO and $NO_2$ gas in the measurement unit was also monitored using an $NO_x$ analytical detector (Horiba Co.: APNA-360) to decrease the concentration error in the measurement process.

BC-curves of SPV-cub measured at room temperature for NO exposure (1 ppm, 800 sccm) and $NO_2$ exposure (1 ppm, 800 sccm) conditions are shown in Figures 5(a) and 5(b), respectively.

There are almost no bias shifts in the 1-ppm NO exposure in Figure 5(a). On the other hand, the bias shift in the 1-ppm $NO_2$ exposure can be clearly observed in Figure 5(b). The bias shift for 1-ppm NO and 1-ppm $NO_2$, respectively, was estimated at 6 mV and 101 mV at a 400nA photocurrent. These results show that SPV-cub has greater sensitivity to 1-ppm $NO_2$ than to 1-ppm NO. Since, as seen in Table 2, the dielectric constant of NO is almost the same as that of $N_2$,[14] it is difficult to detect the difference between NO and $N_2$. On the other hand, the dielectric constant of $NO_2$ exhibits a difference from that of $N_2$, allowing the difference between $NO_2$ and $N_2$ to be measured.

At low concentration exposures, a different sensing performance, which results from the different dielectric constants of NO and $NO_2$, is observed. The bias shift ratio of the 1-ppm $NO_2$ exposure over the 1-ppm NO exposure from the experimental result is almost 20. On the other hand, their bias shift ratio is 27.4 from eq 11, where the dielectric constant of $N_2$ is

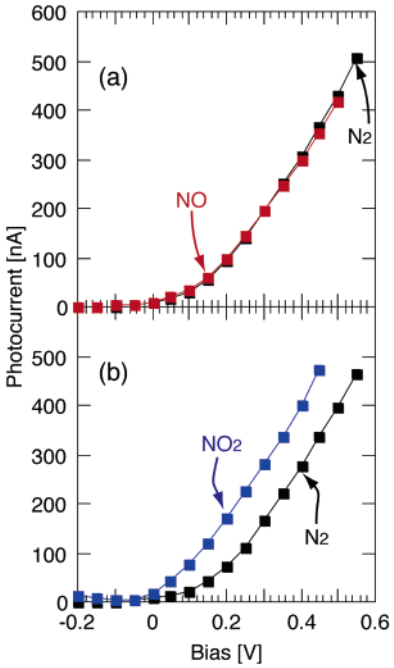


**Figure 5.** BC-curve of SPV-cub sensor in (a) the 1 ppm NO exposure and (b) the 1 ppm $NO_2$ exposure. Closed black, red, and blue squares, respectively, indicate standard (nitrogen) gas, 1 ppm NO gas, and 1 ppm $NO_2$ gas exposure.

used as that of the reference gas (Table 2). This theoretical value is similar to that of the experimental data.

## Conclusions

SPV-type gas sensors with combined self-ordered hexagonal and self-ordered cubic structure mesoporous silica film (SPV-hex and SPV-cub) have been successfully constructed. These sensors have sensitivity to NO and $NO_2$ gas at very low concentrations of 1 ppm to very high concentrations of 50 and 100 ppm. This sensitivity can be explained by the different dielectric constants of the target gases that are physically adsorbed onto the inner surfaces of the mesopores in the self-ordered mesoporous silica film. This physical sensitivity also can be employed to selectively detect other target gases. The high surface area contributes to their high physical sensing performance. Moreover, the sensing performance of the SPV-type sensor depends strongly on the surface area $S_{meso} + S_{micro}$, the dielectric constant, and the charge on the surface. Considering the first parameter, the self-ordered mesoporous silica film is used as an insulating layer to increase the surface area, and the micropores also can be used as a filter to prevent large molecules from entering. Considering the second parameter, the dielectric constant is employed to improve the selectivity of the sensor. Considering the third parameter, the surface charge, which is related to the chemical adsorption or exchange of charge between the surface of the mesopore and the adsorbed gas molecules, can be also employed to improve the selectivity of the sensor that is in development by incorporating transition metals, such as Sn, Ti, V, Zn, W, etc., and the noble metal Pt into the mesoporous film.[20,21] The sensing performance also depends strongly on the mesostructure of the self-ordered mesoporous film. The self-ordered cubic structure mesoporous silica film is more suitable as a SPV-type gas sensor.

## References and Notes

(1) Sberveglieri, G.; Depero, L.; Groppelli, S.; Nelli, P. *Sens. Actuators, B* **1995**, *26*−*27*, 89.
(2) Cantalini, C.; Pelino, M.; Sun, H. T.; Faccio, M.; Santucci, S.; Lozzi, L.; Passacantando, M. *Sens. Actuators, B* **1996**, *35*−*36*, 112.
(3) Depero, L. E.; Ferroni, M.; Guidi, V.; Marca, G.; Martinelli, G.; Nelli, P.; Sangaletti, L.; Sberveglieri, G. *Sens. Actuators, B* **1996**, *35*−*36*, 381.
(4) Zhao, D.; Yang, P.; Melosh, N.; Feng, J.; Chmelka, B. F.; Stucky, G. D. *Adv. Mater.* **1998**, *10*, 1380.
(5) Zhou, H. S.; Yamada, T.; Asai, K.; Honma, I.; Uchida, H.; Katsube, T. *Jpn. J. Appl. Phys.* **2001**, *40*, 7098.
(6) Yamada, T.; Zhou, H. S.; Uchida, H.; Tomita, M.; Ueno, Y.; Ichino, T.; Honma, I.; Asai, K.; Katsube, T. *Adv. Mater.* **2002**, *14*, 812.
(7) Yamada, T.; Zhou, H. S.; Uchida, H.; Tomita, M.; Ueno, Y.; Honma, I.; Asai, K.; Katsube, T. *Microporous Mesoporous Materials* **2002**, *54*, 269.
(8) Schroder, D. K. *Meas. Sci. Technol.* **2001**, *12*, R16.
(9) Zhang, W.; Uchida, H.; Katsube, T.; Nakatsubo, T.; Nishioka, Y. *Sens. Actuators, B* **1998**, *49*, 58.
(10) Sze, S. M. *Physics of Semiconductor Devices*, 2nd ed.; John Wiley & Sons, Inc.: New York, 1981.
(11) Ogawa, M. *J. Am. Chem. Soc.* **1994**, *116*, 7941.
(12) Kundu, D.; Zhou, H. S.; Honma, I. *J. Mater. Sci. Lett.* **1998**, *17*, 2089.
(13) Yamada, T.; Asai, K.; Endo, A.; Zhou, H. S.; Honma, I. *J. Mater. Sci. Lett.* **2000**, *19*, 2167.
(14) *Encyclopaedia Chimica*; Kyouritu Shuppan, Inc.: Tokyo, 1961.
(15) Zhao, D.; Feng, J.; Huo, Q.; Melosh, N.; Fredirckson, G. H.; Chmelka, B. F.; Stucky, G. D. *Science* **1998**, *279*, 548.
(16) Zhao, D.; Huo, Q.; Feng, J.; Chmelka, B. F.; Stucky, G. D. *J. Am. Chem. Soc.* **1998**, *120*, 6024.
(17) Ryoo, R.; Ko, C. H.; Kruk, M.; Antochshuk, V.; Jaroniec, M. *J. Phys. Chem. B* **2000**, 104, 11465.
(18) Jun, S.; Joo, S. H.; Ryoo, R.; Kruk, M.; Jaroniec, M.; Liu, Z.; Ohsuna, T.; Terasaki, O. *J. Am. Chem. Soc.* **2000**, *122*, 10712.
(19) Impéror-Clerc, M.; Davidson, P.; Davidson, A. *J. Am. Chem. Soc.* **2000**, *122*, 11925.
(20) Brian, Y.; Zhou, H. S.; Yamada, T.; Honma, I.; Asai, K. *ChemPhysChem* **2004**, *5*, 261.
(21) Yamada, T.; Zhou, H. S.; Hiroishi, D.; Tomita, M.; Ueno, Y.; Asai, K.; Honma, I. *Adv. Mater.* **2003**, *15*, 511.